Performance assessment of liquid hydrogen pump for the ESS cryogenic moderator system during initial commissioning using helium

H Tatsumoto[1*], A Horvath[1], T Vasilopoulos[1], I Haag[1], and G Ariyoshi[2]

[1] European Spallation Source (ESS) ERIC, Lund, Sweden.
[2] Japan Atomic Energy Agency, Tokai, Japan.

[*]E-mail: hideki.tatsumoto@ess.eu

Abstract. At European Spallation Source (ESS), a cryogenic moderator system (CMS) continuously supplies subcooled liquid hydrogen at 17 K and 1.1 MPa with a parahydrogen fraction exceeding 99.5% to the two moderators. To limit temperature rises across each moderator below 3 K, a flow rate of 250 g/s per moderator is required. The associated pressure drop at the flow rate is estimated to be 100 kPa. Two centrifugal pumps, arranged in series, provide the necessary pump head to sustain the required flow rate of 0.5 kg/s. During preliminary commissioning using helium before hydrogen operation, pump performances were measured at 118 K, 31 K, and 17 K. When expressed in terms of dimensionless expression of head (ψ) and discharge (ϕ) coefficients, all measured data aligned on a single curve, independent of temperature and pump speed. The maximum adiabatic efficiency (η_{max}) was observed around ϕ = 0.029 across all conditions. The efficiency dropped rapidly when the discharge coefficient deviated from this value. A temperature drop to 9.9°C at the pump flange was observed at ϕ = 0.024. The results indicated the pumps should operate within $0.028 < \phi < 0.034$ to maintain the flange temperature above 10°C.

1. Introduction

At the European Spallation Source (ESS), high-energy neutrons produced through spallation reactions are moderated to cold and thermal neutrons using a combination of hydrogen moderators and a light water premoderator, optimized to achieve high cold neutron brightness [1]. The ESS employs two hydrogen moderators positioned above the target wheel, with an estimated nuclear heating of 6.7 kW at a proton beam power of 5 MW. In the future, this configuration will be expanded to four moderators, increasing the total nuclear heating to approximately 17.2 kW [2].

A cryogenic moderator system (CMS) circulates subcooled liquid hydrogen at 17 K and 1.1 MPa, with a parahydrogen fraction exceeding 99.5%, to two moderators, as shown in Figure 1 [3]. A parallel configuration is implemented to ensure the consistent supply of liquid hydrogen at 17 K with a parahydrogen fraction of over 99% to each moderator. Each moderator requires a flow rate of 250 g/s to limit temperature rises across it to less than 3 K, resulting in total circulation flow rates of 0.5 kg/s for the two-moderator configuration and 1.0 kg/s for the planned future four-moderator configuration. The associated pressure drops for these flow rates are

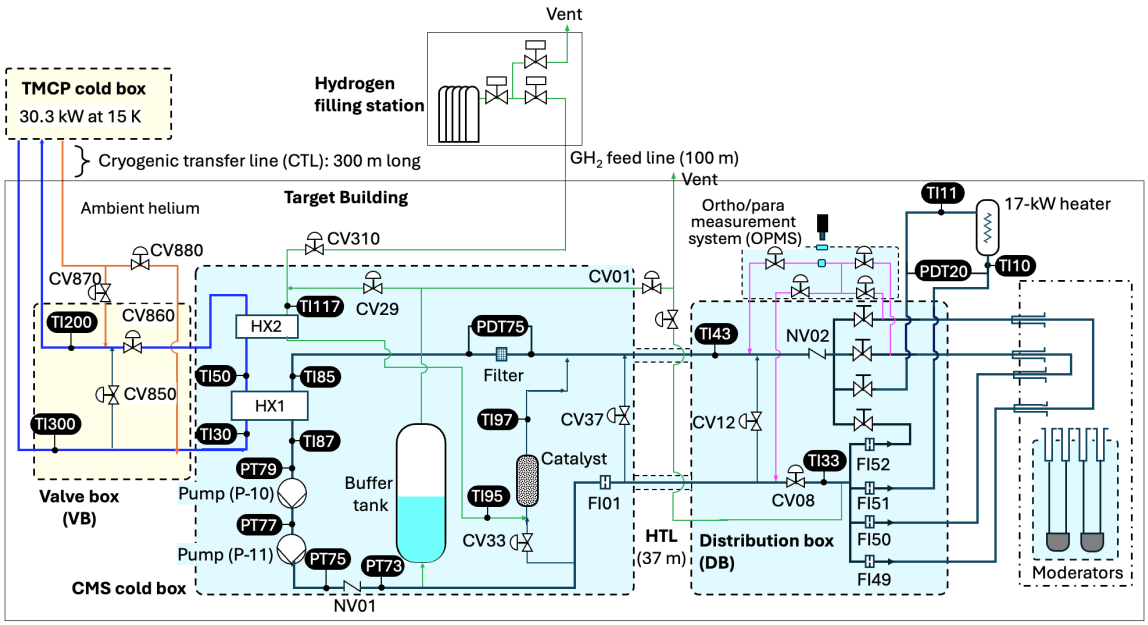

Figure 1. Overview of the ESS cryogenic moderator system (CMS).

estimated to be 100 kPa and 156 kPa, respectively [3]. To overcome these significant pressure drops, two pumps with ball-bearings, arranged in series, are incorporated to provide the necessary pump head at the required flow rates. An ortho-to-parahydrogen catalyst (IONEX® Type OP) with a volume of 35 liters and a grain size of 0.5 mm is installed in a bypass line to achieve equilibrium ortho-to-parahydrogen fraction, as the pressure drop over the catalyst vessel would reach 127 kPa at a flow rate of 1 kg/s [3]. Static and transient heat loads in the CMS are removed via a plate-fin type heat exchanger by a large-scale 20 K helium refrigeration system, which is called the Target Moderator Cryoplant (TMCP), with a maximum cooling power of 30.3 kW at 15 K [4, 5].

The CMS cold box was fabricated in 2020 by the ESS in-kind partner, Forschungszentrum Jülich GmbH (FZJ). A cryogenic test for the cold box using liquid nitrogen was conducted until September 2021 [6], demonstrating that the system met design specifications, including pressure drop, hydrogen pump performance, and pressure control functionality. The CMS installation, excluding connection to the moderators, was completed in May 2024 [7]. During preliminary commissioning using helium prior to hydrogen operation, the mechanical and thermal performances of the hydrogen pumps were evaluated. This paper presents the test results and identifies the optimized operational conditions for the hydrogen pumps.

2. ESS liquid hydrogen pumps

As shown in Figure 2, two ball-bearing type centrifugal pumps arranged in series were designed to circulate subcooled liquid hydrogen at 17 K and 1.1 MPa, overcoming a significant pressure drop of 156 kPa at a flow rate of 1.0 kg/s for the four-moderator arrangement [3]. The pump speeds are adjustable from 1,000 to 14,000 rpm. For the two-moderator and future four-moderator configurations, both pumps operate at rotation speeds of 7,500 rpm and 10,000 rpm, respectively, to achieve the required flow rates. In the event of a pump failure, the remaining pump increases its speed to 10,000 rpm and 13,000 rpm.

Each pump features a closed impeller made of aluminum alloy with a diameter of 95 mm. The pump unit, with a flange diameter of 216 mm, is removable from its housing to allow for ball-bearing replacement every 5,000 operating hours. Thermal baffles, with a height of 104 mm, are arranged vertically from the flange to the rear of the impeller to minimize heat input. An EPDM (ethylene propylene diene monomer) O-ring seal is used, suitable for operation down to -50 °C. The induction motor, located above the flange, is cooled by a 15-20°C ethylene-glycol water mixture flowing at 5.7 L/min. The coolant passes helically through the motor housing from the bottom to top.

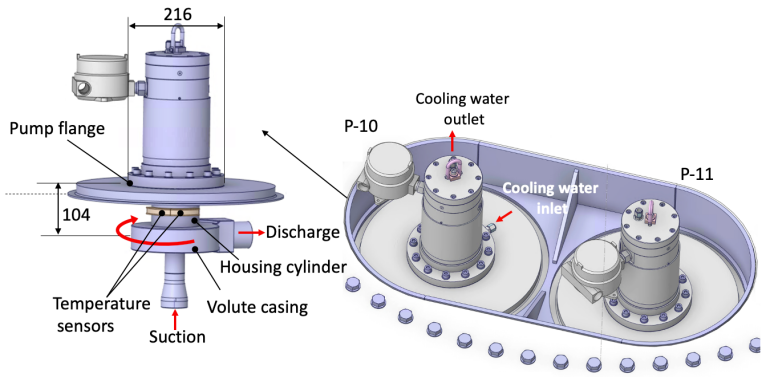

Figure 2. Overview and layout of the liquid hydrogen pumps.

2.1 Pump performance test

Prior to hydrogen operation, CMS commissioning was conducted using helium until December 2024. The CMS cool-down process is divided into three phases: Phase I involves gaseous hydrogen above 36 K, Phase II covers condensation from 36 to 31 K, and Phase III corresponds to liquid hydrogen below 31 K [8]. Due to the cracking pressure of two check valves (NV01 in the CMS cold box and NV02 in the distribution box), the total pressure drop was too high to allow helium to circulate through the moderators at ambient temperature. Therefore, from ambient temperature down to 120 K, helium was circulated via the bypass valve (CV12) in the distribution box, bypassing the moderator distribution lines. During Phase I, the CMS supply temperature was temporarily maintained at 120 K by the TMCP temperature controller until the moderator distribution lines were fully precooled. At the transition from Phase II to Phase III, the CMS supply temperature was held at 31 K. Pump performance tests were conducted at 118 K and 1.0 MPa, and at 31 K and 0.85 MPa, by varying the pump revolution speeds. The pump heads were measured using the pressure transmitters located at the pump inlet and outlet (PT77, PT79, and PT75) by adjusting the bypass valve (CV12) and supply valve (CV08) in the distribution box. Prior to the cooldown, the pressure transmitters PT79 and PT75 were calibrated using PT77 as a reference. Figure 3 shows the measured performance curves for each pump at 118 K and 31 K. As

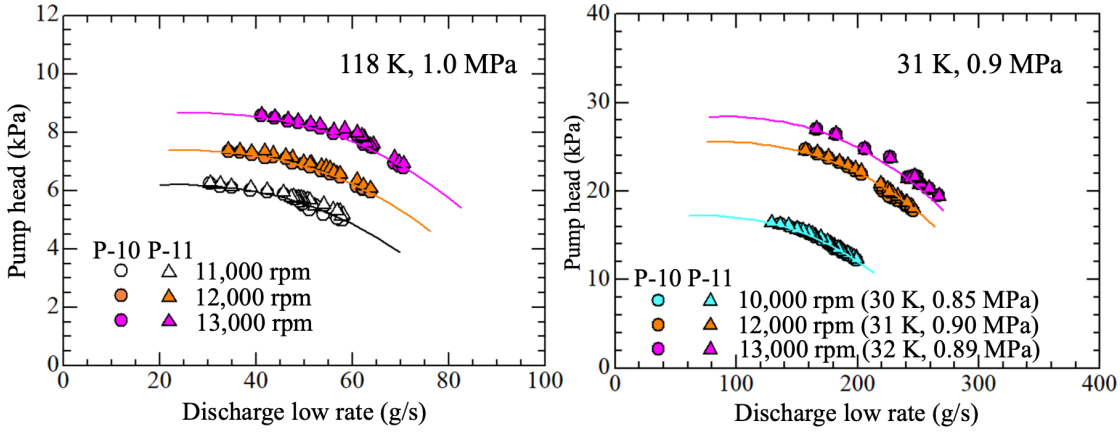

(a) 118 K (b) 31 K

Figure 3. Measured performances during the cool-down process.

the discharge flow rate increased, the pump head decreased monotonically. With higher revolution speeds, the performance curves shifted to the right side on the graph. Both the pump heads and discharge flow rates were higher at lower temperatures. The test results demonstrated that the two pumps exhibited identical performance when operated under the same conditions.

Figure 4 shows the measured performances of each pump at 17.5 K and 0.61 MPa. At a revolution speed of 13,000 rpm, the maximum discharge flow rate of 340 g/s was achieved with both CV12 and CV08 fully open. Subsequently, CV08 was gradually closed to increase the pump head, while the pump flange temperature was maintained above 10 °C, as described below. The maximum pump head reached 35.2 kPa at a discharge flow rate of 252 g/s. The two pumps exhibited identical performance, consistent with the results obtained at 118 K and 31K. Tatsumoto et al. [6] previously measured the pump performance during cryogenic acceptance tests using liquid nitrogen at FZJ following the CMS cold box fabrication and derived a performance curve correlation from the experimental data. The current measurements showed good agreement with the predicted pump performances at each revolution speed, displayed in Figures 3 and 4.

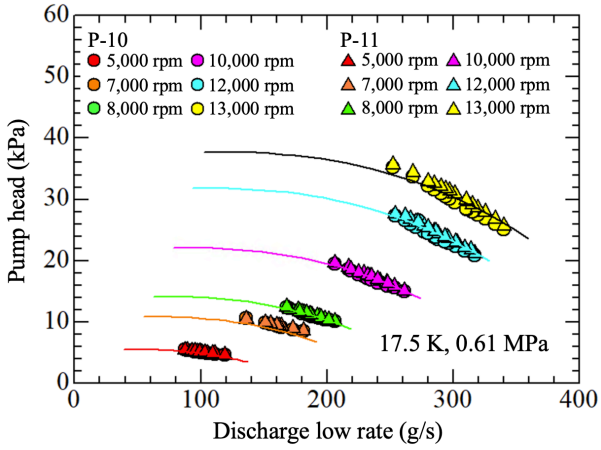

Figure 4. Measured pump performances at 17.5 K.

It is well known that pump performance can be represented using dimensionless parameters: the head coefficient (ψ) and the discharge coefficient (ϕ).

$$\psi = \frac{\Delta P}{\rho {u_S}^2} \tag{1}$$

$$\phi = \frac{\dot{m}}{\rho u_S D^2} \tag{2}$$

where D is the impeller diameter of 0.095 m, $u_s = \pi ND/60$ is the wheel speed, N is the speed of revolution (rpm), ρ is the density, $\dot{m}$ is the discharge mass flow rate, and ΔP is the pump head.

Figure 5 shows the measured non-dimensional pump performance at various temperatures and revolutions. The data include measurements obtained with liquid nitrogen (LN_2) at 78.8 K and 0.51 MPa during the cryogenic test at FZJ in 2021 [6], as well as those obtained with gaseous nitrogen at 121 K and 1.0 MPa during preliminary CMS commissioning [7]. The pump performance curve was derived from the experimental data

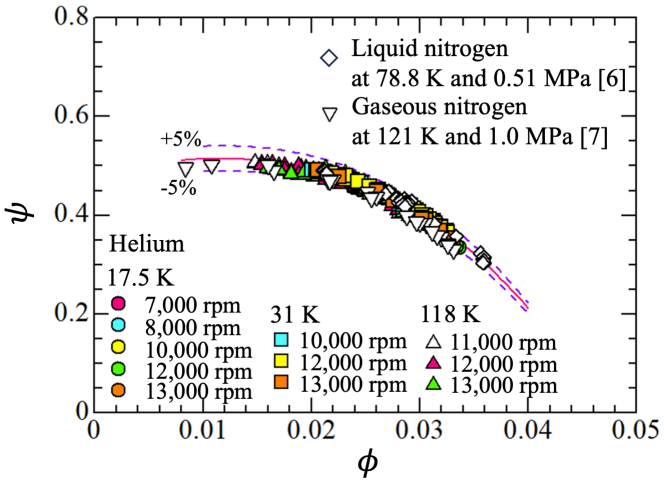

Figure 5. Measured pump performances at 17.5 K.

obtained using liquid nitrogen. It was confirmed that all measured data, regardless of the working fluid, align with the derived performance curve within ±5% errors.

2.2 Heat load measurement

Figure 6 illustrates an example of the P-10 pump behavior, showing the discharge flow rate ($\dot{m}$), pump head (ΔP), housing temperatures (T_h), and estimated heat load (Q) during measurements conducted at 17.5 K and 0.61 MPa with a revolution speed of 13,000 rpm. Following changes in operating conditions, the pump head and discharge flow rate rapidly reach steady-state value. In contrast, the housing temperatures (T62089 for P-10 and T62093 for P-11), whose locations were shown in Figure 7, responded more gradually, requiring over 800 seconds to stabilize. Therefore, heat load measurements were carried out only after the housing temperatures had fully stabilized.

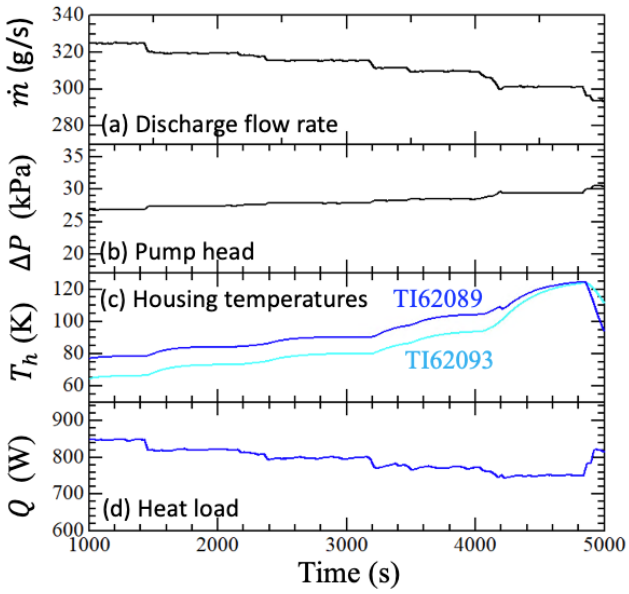

Figure 6. Measured pump performances at 17.5 K.

Figure 8 shows the heat load measurement results for each pump at 17.5 K and 0.61 MPa, plotted as a function of the discharge coefficient. The heat load increased with rising revolution speeds. Notably, the minimum heat load consistently occurs at a discharge coefficient of approximately 0.0292, regardless of the revolution speed. Figure 9 shows the measured housing temperatures of each pump as a function of the discharge coefficient. Similar to the heat load behavior, the housing temperatures peak at discharge coefficient of approximately 0.0292, independent of the revolution speed. The decrease in housing temperature becomes more significant when deviating from this discharge coefficient. Beyond this point, the housing temperatures rapidly drop to approximately 50 K. This behavior is assumed to result from flow induced on the rear side of the impeller, which cools the region between the impeller and flange. In this region, a static temperature distribution is likely formed due to the

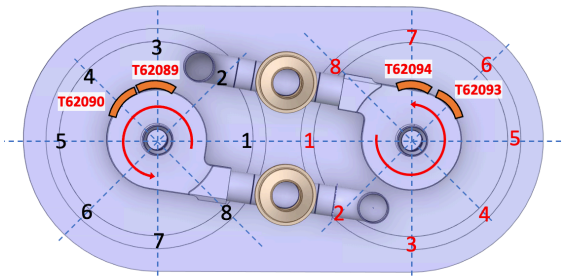

Figure 7. Housing temperature sensor locations.

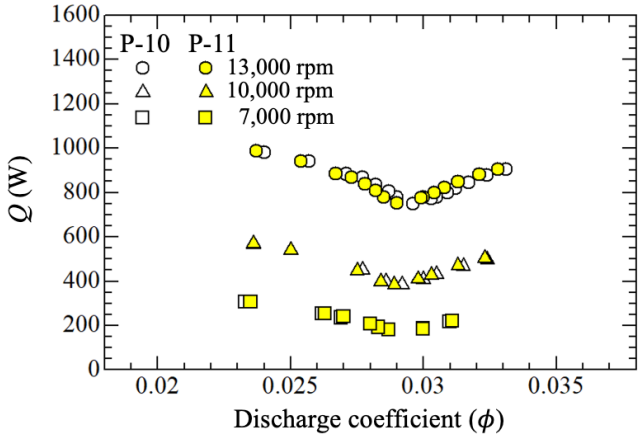

Figure 8. Heat load measurement results at 17.5 K.

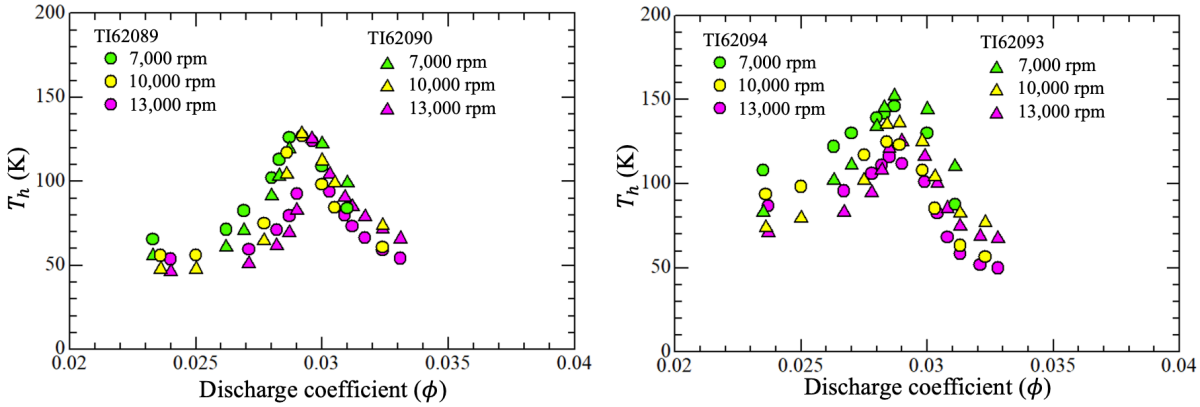

(a) P-10 pump (b) P-11 pump

Figure 9. Measured housing temperatures of each pump as a function of the discharge coefficient.

thermal conductivity within the pump housing. The difference in housing temperature distributions between P-10 and P-11 are considered to result from the sensor locations.

2.3 Adiabatic efficiency

Adiabatic pump efficiency (η) is estimated as follows:

$$\eta = \frac{h_{out} - h_{in}}{h'_{out} - h_{in}} \tag{3}$$

where h is the enthalpy, h' is the enthalpy at isentropic compression and the subscripts "out" and "in" denote the discharge and suction, respectively.

Figure 10 shows the adiabatic efficiency measured at 17.5 K and 0.61 MPa, for revolution speeds of 7,000, 10,000, and 13,000 rpm, plotted as a function of the discharge coefficient. The maximum efficiency consistently occurs at a discharge coefficient of approximately 0.0292, which corresponds to the minimum heat load described in 2.2, regardless of the revolution speed. As the revolution speed increases, the efficiency also improves. The maximum efficiency reaches 0.68 at 13,000 rpm. The efficiency reductions observed when deviating from this optimal discharge coefficient (0.0292) are attributed to the excessive reduction in housing temperature shown in Figure 9.

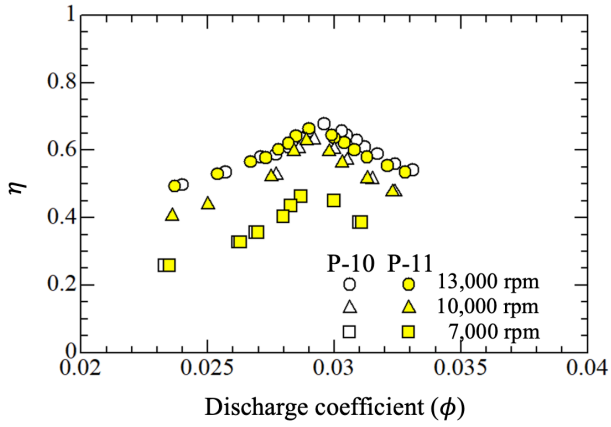

Figure 10. Adiabatic efficiency.

2.4 Pump flange temperature measurement

Figure 11 shows the flange temperatures measured around the circumference of the pump at 17.5 K and 0.61 MPa, for revolution speed of 13,000 rpm. As shown in Figure 7, the measurement locations are numbered in the flow direction, from upstream to downstream within the volute casing. Similar to the trends observed in efficiency and housing temperatures, the flange temperatures also remained close to room temperature at discharge coefficient of approximately 0.0292. A reduction in efficiency was observed when deviating from this discharge coefficient.

For $\phi <$ 0.0292, significant temperature variations around the circumference were observed, with the minimum temperature dropping to 9.9°C. In contrast, for $\phi >$ 0.0292, the temperature variations around the circumference were insignificant, and the flange temperatures remained above 14°C.

Figure 12 shows the flange temperature distributions around the circumference of P-10 and P-11 pumps at 13,000 rpm for each discharge coefficient. The distribution trends differ depending on whether discharge coefficient is below or above 0.0292. For $\phi <$ 0.0292, the minimum flange temperature was observed at location 4, which was situated opposite the discharge pipe, while the maximum flange temperature, close to ambient temperature, was found at location 8, near the discharge pipe. As the discharge coefficient approaches 0.0292, the circumferential temperature difference decrease, and the flange temperatures converge to ambient temperature. When the discharge coefficient exceeded 0.0292, the flange temperature began to decrease again, and the maximum and minimum temperatures shifted to locations 4 and 8, respectively. However, the temperature difference remained relatively small. The housing temperature sensors for the P-10 are installed at locations 3 and 4, while those for the P-11 are at locations 5 and 6, as shown in Figure 7. Since both pumps demonstrated identical performance, the housing temperature distributions around the circumference can be analysed by combining data from both pumps. The locations of minimum and maximum housing temperatures followed trends similar to those of the flange temperature. For $\phi >$ 0.0292, although the housing temperature decreased significantly, falling below 60 K, similar to the behaviour for $\phi <$ 0.0292, the flange temperature differences remained within 2 °C . These performance test results suggest that, for liquid hydrogen operation, the hydrogen pumps

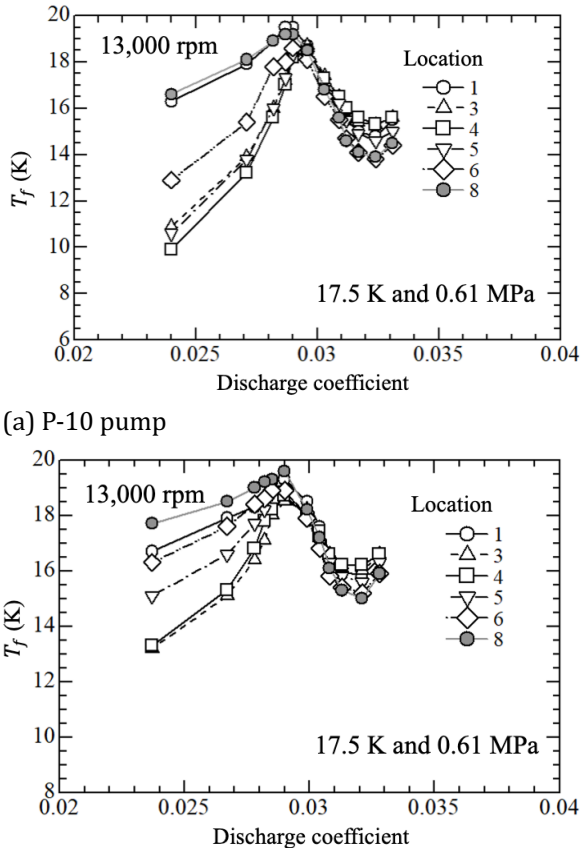

Figure 11. Pump flange temperatures.

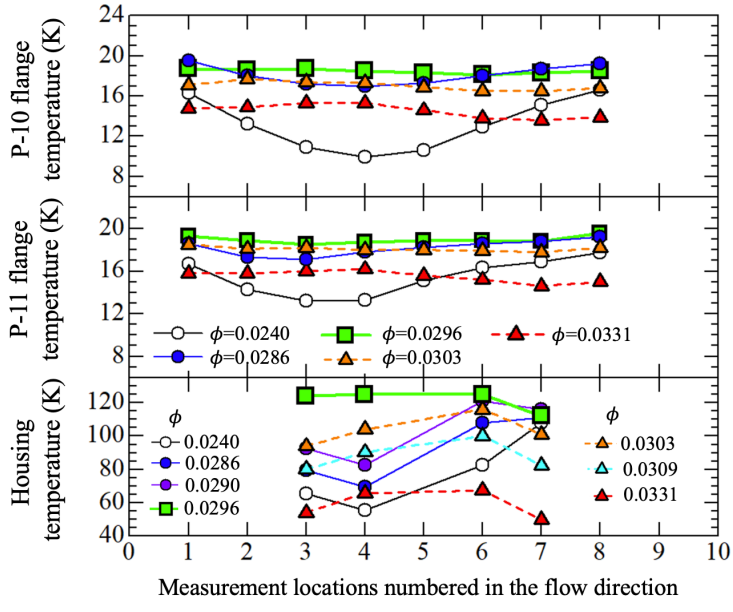

Figure 12. flange temperature distributions around the circumference of the pumps.

should operate under conditions where $\phi > 0.028$, to prevent unexpected flange temperature reductions caused by its higher density, specific heat, and thermal conductivity.

2.5 Measures against the flange temperature reduction

Based on the performance test results, a water-cooled radiator was designed as a countermeasure to maintain the flange temperature at ambient levels and to expand the allowable operational range of the discharge coefficient, as shown in Figure 13. In this system, glycol-water heated by the P-10 pump motor is delivered to its radiator for cooling before being directed to the P-11 pump motor. This circulation helps maintain the flange at ambient temperature.

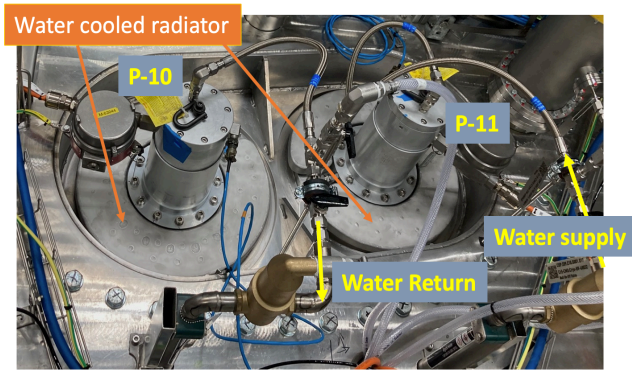

Figure 13. Designed water-radiator to stabilize the flange temperature.

3. Conclusions

During preliminary commissioning using helium prior to hydrogen operation, the mechanical and thermal performance tests of the hydrogen pumps were conducted. The pump performance characteristics, including discharge flow rate and pump head, were measured at 118 K, 31 K and 17.5 K. All pump performance data were successfully expressed using non-dimensional discharge and head coefficients derived from experimental data obtained with liquid nitrogen. As the revolution speed increased, the heat load, which depended on the discharge coefficient, increased accordingly. The minimum heat load and maximum efficiency were consistently observed at a discharge coefficient of approximately 0.0292, regardless of the revolution speed. This behavior was attributed to reductions in housing and flange temperatures, resulting from flow induced on the back side of the impeller. The results demonstrated that pump thermal performances could be effectively characterized by the discharge coefficient. Furthermore, a water-cooled radiator was designed as a countermeasure to mitigate excessive flange temperature reduction during liquid hydrogen operation.

References

[1] Andersen K, Bertelsen M, Zanini L, Klinkby E B, Schönfeldt T, Bentley P M and Saroun J 2018 *J. Appl. Cryst.* **51** pp264-281
[2] Bessler Y, Henkes C, Hanusch F, Schumacher P, Natour G, Butzek M, Klaus M, Lyngh D and Kickulies M 2017 *IOP Conf. Ser.: Mater. Sci. Eng.* **171** 012131
[3] Tatsumoto H, Lyngh D, Bessler Y, M Klaus, Hanusch F, P Arnold and H Quack 2019 *IOP Conf. Ser: IOP Conf. Ser.: Mater. Sci. Eng.* **755** 012101
[4] Arnold P, Hess W, Jurns J, Su X T, Wang X L and Weisend II J G 2015 *IOP Conf. Ser: IOP Conf. Ser.: Mater. Sci. Eng.* **101** 012011
[5] Tatsumoto H, Arnold P, Boros M, Horvath A, Segerup M, Tereszkowski P, Arriagada J and Huber R 2024 *IOP Conf. Ser.: Mater. Sci. Eng.**1301** 012131.*
[6] Tatsumoto H, Beßler Y, Rosenthal E, Arnold P, Kickulies M, Boros M, Horvath A, Segeup M, Tereszkowski P, and Lyngh D 2023 *Proc. 28th Int. Cryo. Eng. Conf. and Int. Cryo. Mater Conf.* Hangzhou, China pp.133-140.
[7] Tatsumoto H, Horvath A, Arnold P, Segerup M Tereszkowski P Arriagada J 2025 *Conf. Ser.: Mater. Sci. Eng. **1327** 012032*
[8] Tatsumoto H, Arnold P, Boros M and Horvath A 2024 *IOP Conf. Ser.: Mater. Sci. Eng. **1301** 01208*